3 Simulation

3.1 Advanced Ignition Modelling for Pre-chamber Combustion in Lean Burn Gas Engines

Evgeniy Shapiro, Irufan Ahmed and Nick Tiney

Abstract

Lean burn combustion systems present a viable route to emissions reductions. However, sustainable and conrolled combustion of lean mixtures can be challenging. Scavenged pre-chamber ignition systems aim to address this challenge by creating favourable ignition conditions close to stoichiometry in the spark region. The main lean charge ignition is then delivered by flame jets propagating through the nozzles connecting the pre-chamber to the cylinder.

Accurate and fast CFD modelling of the mixture formation and early flame kernel development in the pre-chamber are essential for the design of such systems. The initial stages of ignition in spark-ignited engines typically occur at time scales, temperatures and length scales falling outside of the remit of conventional CFD techniques prompting development of specialised ignition models.

A review of the models currently available highlighted a gap in the technology currently available in commercial CFD codes. Simplistic models based on direct energy transfer or fixed temperature kernel development are readily available but these models to not provide an accurate representation of the spark growth. More complex models are also available which are based on complex chemistry/turbulence interaction. While these models can provide accurate solutions they require standalone chemistry solvers or spatial temperature distribution calculations. These can be time consuming to solve, making the models less than ideal for simulations in a production environment.

A novel spark model has been developed by Ricardo and implimented into the CFD software VECTIS, allowing for an accurate specification of the spark-ignition process. The model covers all stages of spark discharge from breakdown and the formation of the initial kernel and includes a predictive model for the initial flame kernel size. The flame kernel evolution is computed via a 1D variable temperature model incorporating plasma physics with two-way coupling with 3D CFD. The detailed chemistry effects are included through flame speed and mixture properties tabulation.

This paper illustrates the principles and applications of the developed model. The model is then applied to the analysis of a novel pre-chamber ignition system and the results are compared with measurement data. A study is performed to investigate the sensitivity of the results to the input parameters within the spark ignition model.

1   Introduction

Road transport in Europe is required to be substantially more efficient by 2020+ with the target of obtaining sustainable mobility, reducing global green-house gas (GHG) emissions such as carbon dioxide (CO2) and reducing local impact emissions such as soot, NOx and unburnt hydrocarbons.

Electrification is at the forefront of the carbon emissions reduction effort and while this technology can provide vehicles which do not emit CO2 from the vehicle themselves, there are other challenges such as battery range vs charging infrastructure/time to contend with. In the short to medium term, a large amount of the targeted improved efficiency will still need to come from the improvement of the energy efficiency of the internal combustion engine.

One approach to reduce the CO2 emissions is to look at alternative low carbon fuels. Natural gas and Compressed Natural Gas (CNG) can be used reduce the carbon emissions compared to traditional gasoline engines but still provide comparable performance.

CNG has several advantages. CNG reserves are greater than oil and on a like for like comparison it is significantly less expensive than gasoline at today's prices. Of all the fossil-based fuels, CNG has the greatest potential for reducing GHG emissions [1]. It is more resistant to knock which makes it ideal for boosting and downsizing. Higher compression ratios can be used to improve efficiency and further reduce CO2 emissions. Additionally, a renewable version of CNG, biogas or biomethane, can achieve carbon neutral fuel classification if produced by biomass or liquid manure [2].

In addition to its natural tendency to reduce CO2 emissions, further efficiencies can be gained when lean burn combustion is employed. By running the engine lean, significant efficiency improvements can be achieved due to reduce heat losses, reduced exhaust losses and a higher compression specific heat ratio.

However, there are also drawbacks to running the engine lean which must be overcome. High cycle to cycle variations and high unburnt hydrocarbons can occur due to the lean flammability limit. These problems have been shown to be functions of the ignition system and combustion speed/duration. One method to avoid these issues is to use a pre-chamber ignition system which can provide large ignition energy into the main combustion chamber via distributed ignition points which ignite the main lean pre-mixed charge more efficiently.

The pre-chamber approach allows for the generation of near stoichiometric conditions and enables control over the turbulence generation close to the spark plug, improving initial combustion and thus cycle to cycle variation. Once the spark ignites the pre-chamber, the main combustion chamber is then ignited by the flame jets as they exit the pre-chamber nozzles.

While there has been lots of research into pre-chamber design for large, heavy duty applications, comparatively little has been done for smaller automotive applications at high compression ratios.

The research and development of such a system is one of the objectives of the Horizon 2020 GasOn project. The GasOn target is to extend the lean limit of operation in natural gas engines to Diesel-like compression ratios [3]. The full GasOn project investigates numerous pre-chamber designs and operating conditions but the initial requirement was the development of a new ignition model to prediction of the initial spark ignition and its growth and propagation through the pre-chamber. This paper looks at the modelling of this spark ignition using the computation fluid dynamics software VECTIS and investigates the sensitivity of the model implemented to modelling parameters.

Accurate modelling of the initial stages of spark ignition is essential for the overall accuracy of the simulations. The Dynamic Discrete Particle Model (DDPIK) developed at Ricardo [5,13] covers all stages of the spark from the point the power is supplied by the ignition coil to the transition of the flame kernel supported by the discharge to a fully developed turbulent flame.

The model for the spark discharge stage in isolation has been previously validated against academic experiments [5]. The complete simulation methodology reported in this paper combining the spark model and the RANS combustion model within Ricardo VECTIS CFD solver has been validated against Rapid Expansion Compression Machine (RCEM) measurements [13] and Large Eddy Simulation combustion models [14]. Furthermore, the complete model has demonstrated good accuracy when applied to the pre-chamber lean operation natural gas engine development with high compression ratio within Horizon 2020 GasOn project [4, 6].

However, in the absence of a detailed spark characterisation under precise conditions of interest and optical access measurements close to spark position, which in the case of pre-chamber engine development remains quite challenging, a number of model parameters remain uncertain. These uncertainties are not fully resolved by the extrapolation of information obtained from validation using stand-alone spark measurements under low pressure quiescent conditions and optical access measurements in different applications. In the present paper the modelling uncertainties are discussed and the effects of the modelling parameters and discretisation approach onto predictions obtained for flame propagation in a pre-chamber mounted on an RCEM are investigated using a validated set-up reported in [13] as a starting point.

2   Validation case description

To validate the spark ignition model, experimental data has been obtained from an optical Rapid Compression Expansion Machine (RCEM). This experiment and methodology is fully described in [13]

This base engine geometry is used throughout, with a single pre-chamber design used in the work presented here. The geometry has an 84mm bore with a stroke length of 249mm. An optical access piston is used with a top hat profile. The top hat shape has a diameter of 52mm and a depth of 2.2mm.

The model of RCEM has then been constructed in VECTIS CFD. The geometry of the RCEM is illustrated in Figure 1.
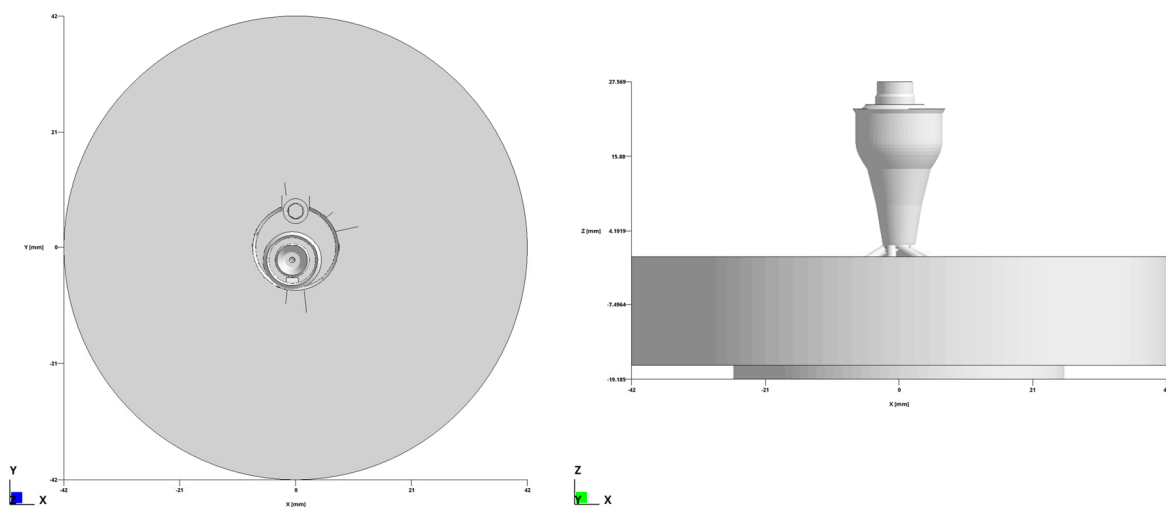

Figure 1: RCEM Geometry

The pre-chamber investigated is shown in Figure 2. The geometry has an effective volume of 1.7e-6. The effective volume is not including the volume of the nozzles but just the volume of the chamber itself. It has 7 nozzles which join the pre-chamber at a tangent. Each nozzle has a diameter of 1.5mm. The nozzle angle with respect to the bore axis is 64.5deg. The shape has been developed at VW through numerical optimisation focussing on mixture homogeneity and ignitability using VECTIS CFD tool within the GasOn project [4,13].
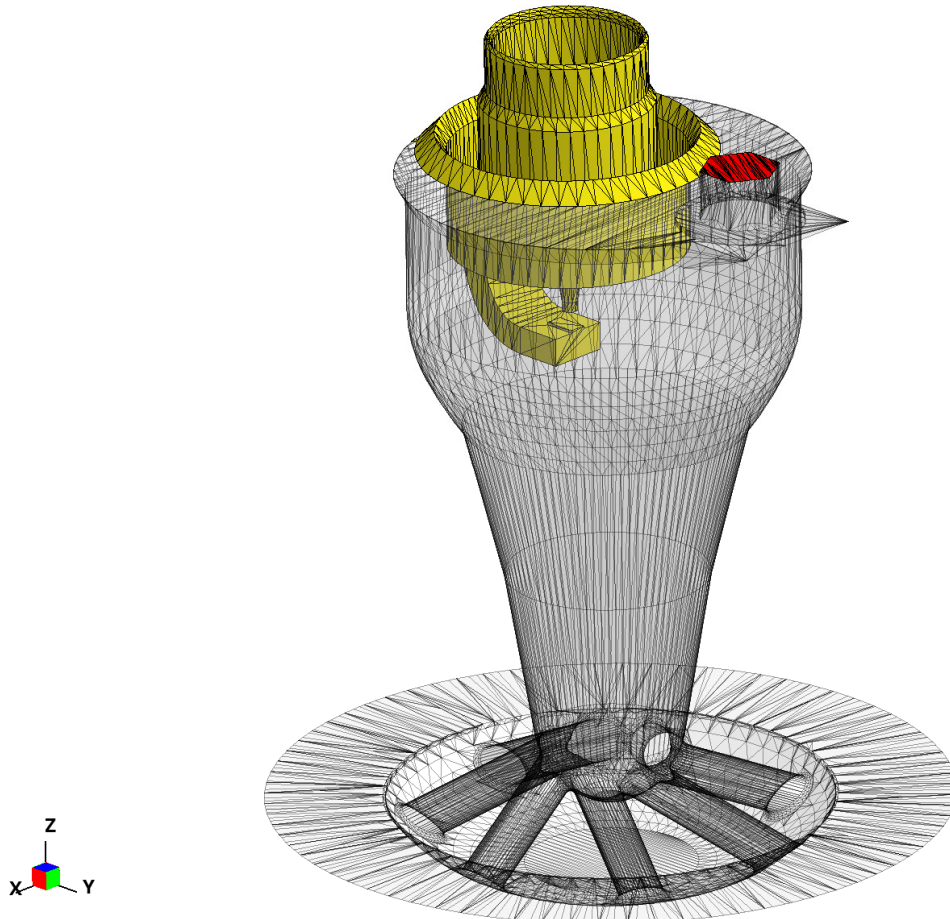
Figure 2: Pre-chamber PC-A Geometry

The RCEM operation is assigned a nominal RPM of 600 which maps bottom dead centre of the RCEM stroke to 540 degrees CA. The simulations are started from quiescent flow conditions with pressure, temperature and composition initialised based on the experimental data at 37 ms bTDC (-133.2 deg CA).

Four combinations of air-fuel mixing are simulated. For each case the mass of fuel injected and the injection duration is varied. The fueling and spark timings of the simulations are given in Table 1

Table 1: Fueling and spark timing

Case	Mass	Start of injection	Injection duration	Spark timing
	mg	CA. deg.		
1	0.9	645.7	18.0	708.8
2	1.2	646.5	23.4	708.8
3	1.5	647.1	28.8	708.7
4	1.7	647.3	34.2	708.7

Initial conditions for the simulations for temperature and pressure are also taken from experiment. The initial conditions used are shown in Table 2.

Table 2: Simulation initial conditions

Case	Temperature	Pressure
	K	Pa
1	380.2	136978
2	389.2	141551
3	396.2	139407
4	392.0	142369

The models and parameters used for combustion modelling in all cases are given in Table 3.

Table 3: Base Simulation models and parameters

Model/parameter	Value
Combustion model	G-equation/RTZF
Laminar flame speed	Metghachi & Keck modified
Turbulent flame speed	Herweg and Maly
G-equation re-initialisation	Geometric with smoothing

For the spark ignition, there are five base inputs which are listed in Table 4.

Table 4: Spark model and parameters

Model/parameter	Value
Spark model	Dynamic DPIK
Breakdown energy	0.1mJ
Effective power	210W
Kernel particles	20000
Spark duration	1.8ms
Burnout radius	1.1mm

The spark duration is defined based on measurement data and is fixed to 1.8ms based on a study of similar spark [25]. The remaining spark parameters will be investigated for model sensitivity.

3   Model formulation and investigated parameters

Accurate modelling of the initial stages of spark ignition is essential for the overall accuracy of the simulation. The Dynamic Discrete Particle Model (DDPIK) developed at Ricardo [5,13] covers all stages of the spark from the point the power is supplied by the ignition coil to the transition of the flame kernel supported by the discharge to a fully developed turbulent flame. To detail the uncertainties inherent in the modelling, it is essential to consider the inputs required for every part of the model.

Firstly, consider the predictive model for the initial radius and temperature of the flame kernel. The estimate of radius at the end of the breakdown of the spark discharge is critical for the correct initial state of the energy balance.

The model employed in DDPIK is an extension of the two-stage breakdown model proposed in [7,8]. The breakdown occurs over the first ~10ns since the initiation of the discharge. At this point a cylindrical plasma channel is formed between the electrodes with the pressure $P_{bd} \sim 20 - 30 MPa$ and temperature corresponding to completely dissociated and ionised plasma in a state approaching thermal equilibrium [8, 15, 11]. Due to the extremely rapid nature of this process, the approach proposed in [8] considers that the breakdown energy E_{bd} is supplied instantaneously, followed by an expansion of the activated volume of the plasma to equilibrate the pressure with the surrounding ambient in a shock wave process. Applying energy conservation over the two stages of the breakdown process results in the following expression of the breakdown radius [8,5]:

$$r_{bd} = \sqrt{\frac{\gamma - 1}{\gamma} \cdot \frac{E_{bd}}{P\pi l \left(1 - \frac{T + LHV/c_p}{\left(\frac{1}{\gamma}(T_{bd} - T) + T\right)}\right)}} \quad (1)$$

The above expression builds on the theory of [8] by including the chemical energy released in the oxidation of fuel present in the activated volume through the lower heating value (LHV) term. In this expression, the parameters of the ambient are the result of a 3D CFD simulation with a low uncertainty level. The break-down temperature, T_{bd}, is well defined. It has been observed that it has the upper limit in the range of $T_{bd} \sim 60000K$, due to the high energy barrier of the third ionisation level of nitrogen [12], which does not change with the flow conditions or mixture composition as long as nitrogen remains the dominant component. The definition of the breakdown energy is more uncertain. This value depends on the ambient conditions and in practice it is not known a-priori. Measurements reported by Rivin et. al. [9] indicate energy less than 1mJ with a spark plug gap of 0.8mm for premixed air/methane at 0.25MPa. The theoretical model of [7] points to breakdown energies <1mJ for the activated plasma channel diameter of 40μm. Maly and Herweg [16] refer to levels of 0.3-1mJ in commercial ignition systems with a minimum energy of 0.3mJ required for breakdown in a 1mm spark gap at 1bar.

After the breakdown, the arc and glow discharge stages follow. In the arc stage, temperatures are in the range 4,000-10,000K, and are dominated by dissociation processes. The glow discharge rate is characterised by temperatures just above the adiabatic flame temperature [11].
After the breakdown stage, a complete simplified 1D model can be formulated in terms of the conservation of mass and energy as follows [5,13]:

$$\begin{cases} \dfrac{dr_k}{dt} = \dfrac{\rho_k}{\rho_u} S_b + \dfrac{r_k}{3}\left(\dfrac{1}{R_k T_k}\dfrac{d(R_k T_k)}{dt} - \dfrac{1}{P_u}\dfrac{dP_u}{dt}\right) \\ \dfrac{dT_k}{dt} = \dfrac{Q}{\frac{4}{3}\pi r_k^3 \rho_u}\dfrac{\gamma_k - 1}{\gamma_k}\dfrac{T_k}{R_u T_u} + \dfrac{3}{c_{p,k} r_k}\left(LHV - \left(c_{p,k}T_k - c_{p,u}T_u\right)\right)\dfrac{\rho_k}{\rho_u}S_b + \dfrac{\gamma_k - 1}{\gamma_k}\dfrac{T_k}{P_u}\dfrac{dP_u}{dt} \end{cases} \quad (2)$$

Where subscripts „k" and „u" refer to kernel and unburnt side of the flame front respectively and in the usual notation R is the gas constant, ρ is the gas density, c_p is the specific heat capacity and γ is the adiabatic index. P represents ambient pressure, Q

is the effective spark power and Sb is the cumulative burn rate comprising turbulent flame speed S_T and the plasma expansion speed:

$$S_b = S_T + \frac{Q}{4\pi r_k^2 \rho_u (c_{p,k} T_k - c_{p,u} T_u)} \quad (3)$$

S_T is modified to account for curvature of the flame:

$$S_T^* = S_T - \frac{2}{r_k}\left(\frac{\nu}{Pr} + 0.28l_{ft}u'\right) \quad (4)$$

where Pr and ν are laminar Prandtl number and dynamic viscosity and u' is the turbulent velocity. The flame brush thickness of the spark flame front l_{ft} is approximated based on the time since ignition and the local turbulent properties ([5]).

The basic turbulent flame speed uses the expression proposed by [11]:

$$\frac{S_T}{S_L} = 1 + A\left(\frac{u'}{u' + S_L}\left(1 - exp\left(-\frac{r_k}{l_I}\right)\right)\left(1 - exp\left(-\frac{(u' + S_L)t}{l_I}\right)\right)\right)^{\frac{1}{2}}\left(\frac{u'}{S_L}\right)^{\frac{5}{6}} \quad (5)$$

Where $l_I = u'^3/\epsilon$ is the integral time scale and S_L is the laminar flame speed.
The 1D model is coupled to 3D CFD using an approach similar to the one proposed in [10] with the kernel front discretised using individual particles randomly distributed on the surface of the spherical flame kernel which is allowed to move with local flow velocity. The particle positions are used to sample the 3D solution for the unburnt quantities required for the 1D model and at the same time particle density is used to distribute the reaction rate source to 3D computational cells.
It is important to note that the kernel radius and temperature are tightly coupled through the system of Equations 2 and temperature must be appropriate for the radius of the kernel. Models which do not take the variation of temperature with time into account (e.g. [10, 20]) should select the kernel temperature carefully to avoid unphysical values of the plasma velocity. For example, using adiabatic flame temperature as the kernel temperature (e.g. [20]) in Equation 2, clearly results in plasma speed increasing away from stoichiometry, where the adiabatic flame temperature decreases.
The 1D model is computed in a coupled manner until either the spark discharge completes, or the kernel reaches the sustainable flame length scale. The sustainability of the kernel has two criteria. Firstly, its radius must exceed the integral length scale of turbulence l_I. Secondly, it should be self-sustained at this stage, i.e. the diffusion of the turbulent flame front should not exceed the flame propagation speed at the kernel surface. The latter criterion can be expressed [19] as:

$$R_c > \frac{2}{S_T}\left(\frac{\nu}{Pr} + 0.28l_{ft}u'\right) \quad (6)$$

Some of the uncertainties in the 1D flame kernel model are familiar from other aspects of modelling methodology for the internal combustion engine. For example, both the turbulent flame speed and the flame brush thickness depend on the integral length

scale, which can be challenging to predict in simulations using Reynolds-Averaged Navier Stokes (RANS) turbulence modelling (e.g. [17]).

The expression for the turbulent flame speed in its fully turbulent form introduced substantial modelling assumptions (e.g. [18]). The main modelling parameters which are a subject of uncertainty in Equation 2 are the effective spark power and the critical radius of transition.
The power transferred to the plasma is a function of time and rapidly varies from $O(10^5)$ to $O(10)$W over the time interval between end of the breakdown stage and end of the glow stage of the discharge. In the absence of detailed measurement data the effective average spark power can be considered as a model tuning parameter.

Note, that there are in effect two critical parameters for the kernel radius. R_c given by Equation 6 corresponds to flame diffusion driven by turbulence generated by the flame front itself. At the same time, the kernel is embedded in the external inhomogeneous turbulent field. For the kernel to be sustainable, it's size should exceed the integral length scale of this turbulent field. This critical radius R_b is subject to uncertainty in terms of the turbulence modelling. Furthermore, the definition. $R_b \sim l_I = u'^3/\epsilon$ provides a correct functional dependence, but the uncertainty in the coefficient of proportionality means that the actual value can be treated as a tuning parameter as well. For example, Tan and Reitz suggest the following definition of the critical radius:

$$R_b = C_T C_\mu^{0.75} k^{1.5}/\epsilon \ (7)$$

[10], with the tuning constant $C_T = 1 - 5$. The length scale definition used in the DDPIK model corresponds to a constant $C_T = 3.3$ in the formulation of [10].
Errors in the solution can also be introduced by the discretisation of the 1D problem. The implementation in VECTIS employs a 1st order accurate discretisation of Equation 2 based on the local Courant number. The space discretisation is given by the number of particles used to sample the 3D solution.

The remaining parts of the CFD set-up follow VECTIS default approach. The realisable k-e model [21] is used with a first order in time, second order in space pressure-correction solver. Based on a grid sensitivity study, a uniform mesh size of Δx=0.18mm was used in the pre-chamber with 0.94mm mesh in the cylinder. The G-equation combustion model is used with a constant A=2.75 in the fully turbulent form of Equation 5.

The baseline case employed 20000 particles with the first 0.2 degrees of the simulation conducted with a Courant number of 0.1, increasing to 1 thereafter. The effective power was set to 210W, with a break-down energy of 0.1mJ and a breakdown temperature of 60000K [5, 13]. The transition radius was estimated a-priori to be 1.1mm based on experience with previous simulations.

The range of the parameters which have been investigated are summarised in Table 5.

Table 5: Simulated cases

Parameter	Minimal value	Maximum value
Effective Power (W)	1	210
Number of particles	1000	20000
Breakdown energy (mJ)	0.1	1
Transition radius (mm)	0.8	1.4
Courant number	0.1/1	0.1/4

To simplify the comparison of the RCEM set-up with engine cases, where appropriate the timings of the RCEM operation have been converted to degrees of crank angle using 600 rpm speed based on the RCEM compression cycle time. The averaging of reported quantities is performed in the volume of the pre-chamber and the spark volume comprised of a sphere centred on the spark plug gap with a 3mm radius.

4   Results and discussion

Figure 3 illustrates the flow and turbulence quantities in the spark region for 0.9mg injection, just before the ignition at -11.15deg. Here the length scale is evaluated using $C_T = 1$ in Equation 7. The velocity and turbulent velocity distributions illustrate the flow structure driven by the inclined nozzles of the pre-chamber which result in a wall-attached spiral jet flow. The spark gap is shielded by the electrodes and features low velocities and moderate turbulence levels creating conditions beneficial for ignition. The local mixture is close to stoichiometry. Note that the turbulent length scale is very close to the initial radius typically assumed in the models which do not cover breakdown conditions (e.g. 0.5mm in [10]).
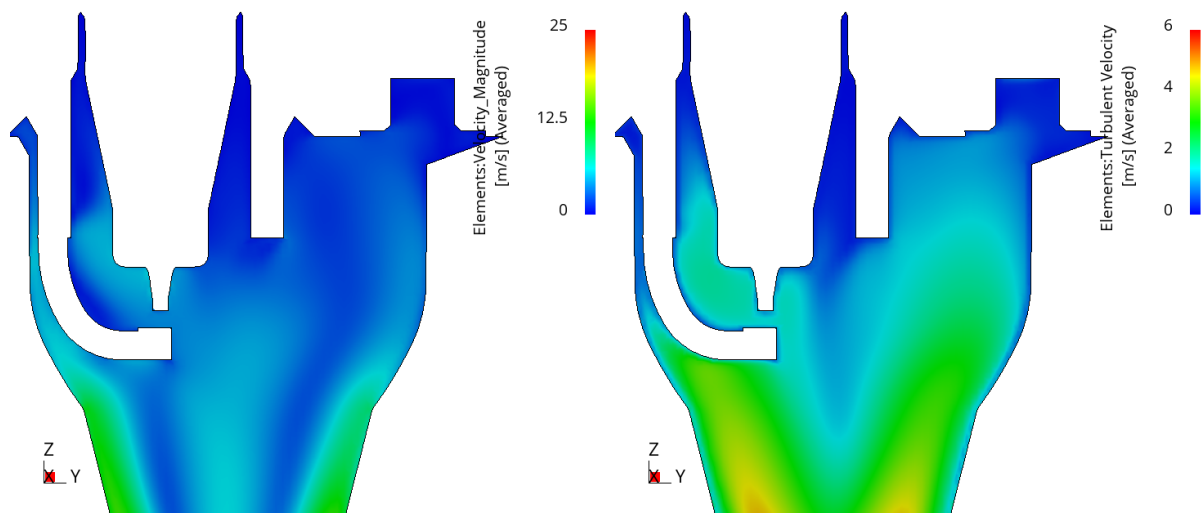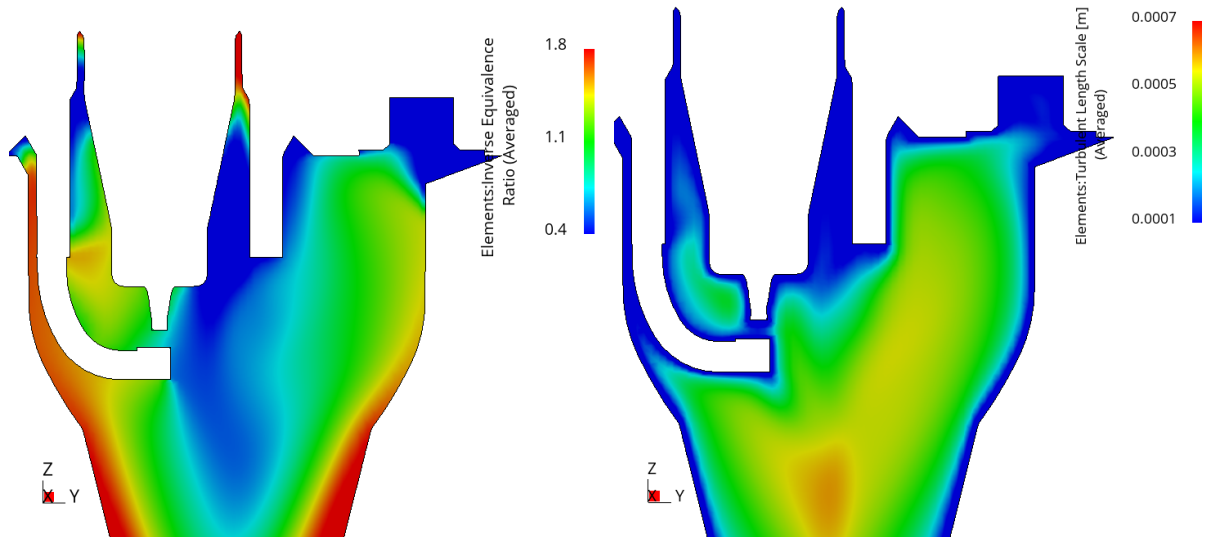
Figure 3: Velocity, turbulent velocity, inverse equivalence ratio and turbulent length-scale near spark plug gap for m=0.9mg injection, at -11.15deg
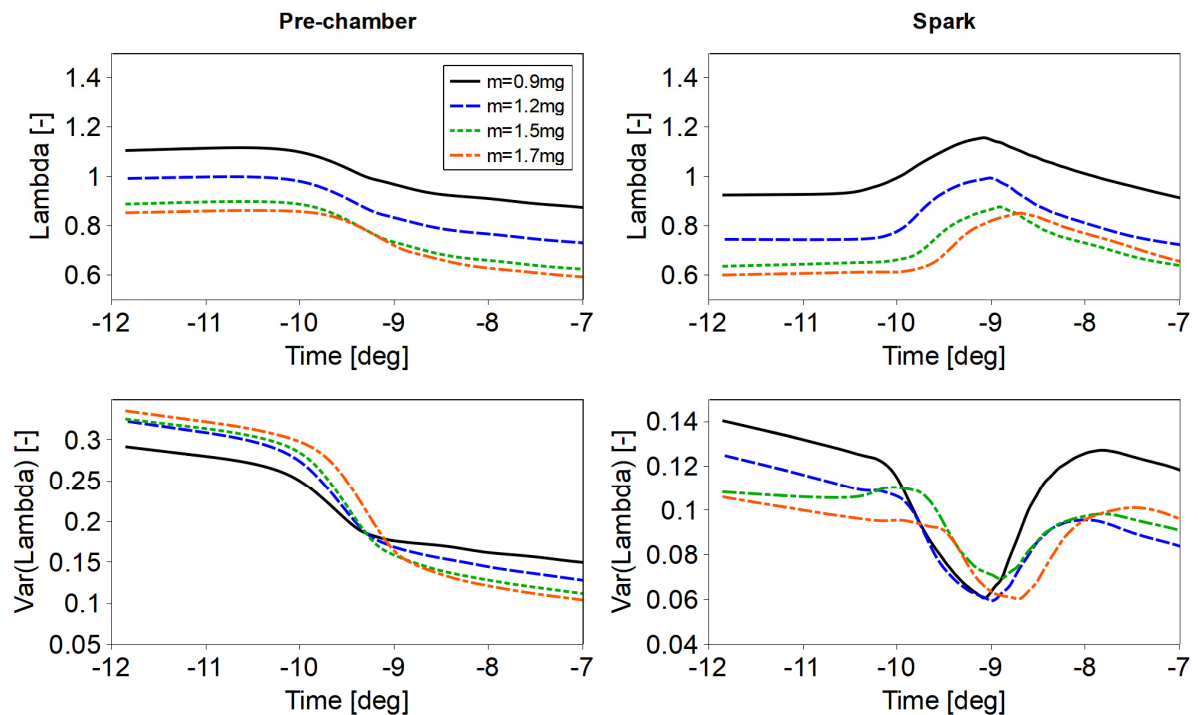

Figure 4: Pre-chamber and spark region mixture composition

Figure 4 illustrates the composition of mixture and its homogeneity in terms of the average values of λ within the pre-chamber and the spark volumes. As could be expected, an increase in the injection mass leads to an increase in the equivalence ratio in both control volumes. Longer injection timings increase inhomogeneity levels in the pre-chamber. However, the effect on the spark volume is opposite. The results indicate that when controlling the total injected mass, it is beneficial to target values slightly leaner (~10% in the investigated case) than estimated stoichiometry based on the pre-chamber volume and density.

An interesting observation is that while the spark volume is always richer than the pre-chamber on average, the actual difference of the average λ between the two volumes at the point of ignition does not change significantly with the injected mass (Figure 5).
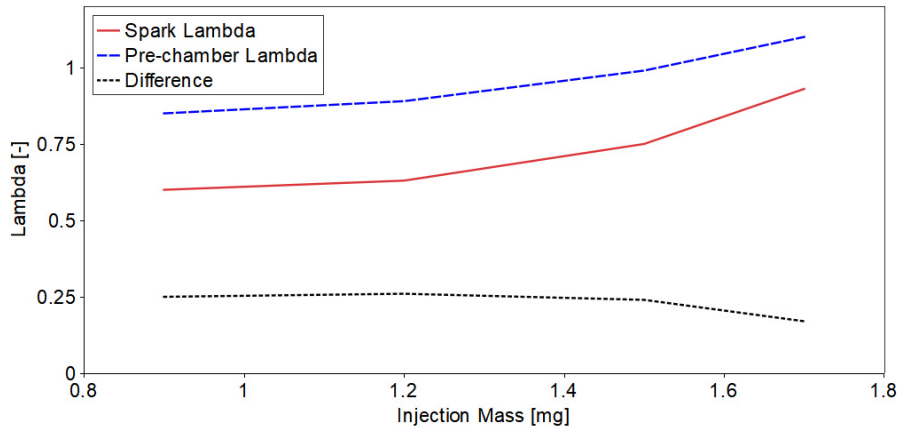

Figure 5: Pre-chamber and spark region mixture composition at ignition point

The integral length scale and turbulence levels at the spark location and in the pre-chamber up to the ignition time are illustrated in Figure 6 for a representative injection case with baseline model parameters. The spark region is less turbulent due to the sheltering by the spark body. The actual integral length-scale is lower than the a-priori estimation.
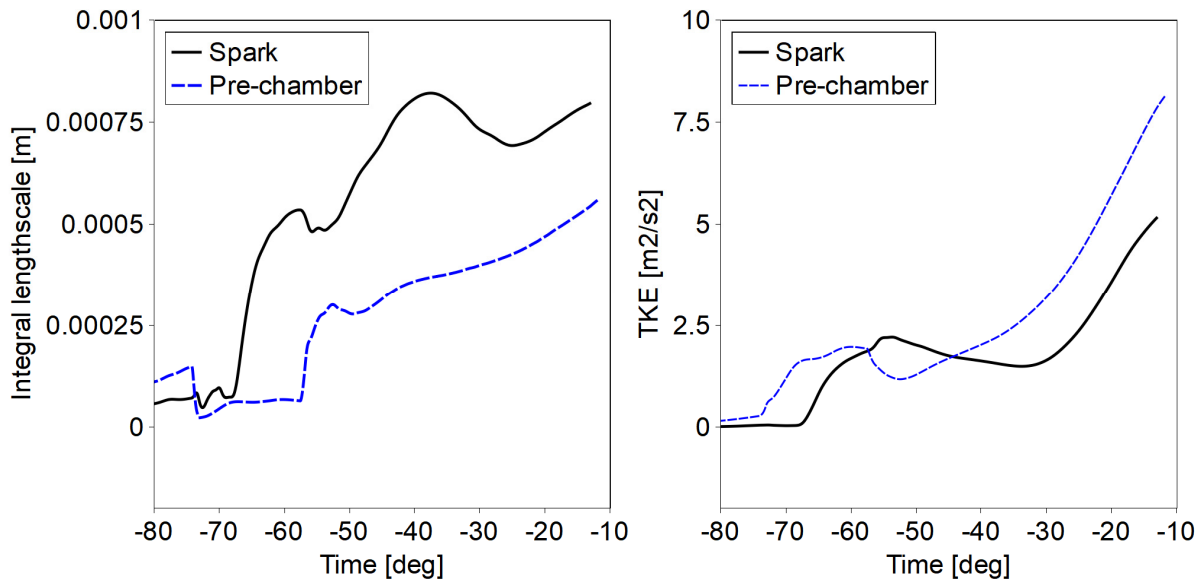

Figure 6: Integral lengthscale evolution (injected mass m=0.9mg, injection timing: -74.3- -56.3deg)

Figure 7 shows the evolution of the kernel radius, critical parameters and the kernel temperature. As the kernel grows, the turbulent component of the flame speed becomes much greater than the laminar component and the turbulent flame brush thickness l_{ft} and the critical radius R_c become identical. The kernel radius for this case grows much faster than the flame brush thickness and as a result, no quenching is

observed. The temperature relaxes over the first ~20μs and becomes close to the adiabatic flame temperature, which is in line with the behavior reported in other studies (e.g. [11]).

The kernel radius at this point is ~0.5mm, which is the appropriate initial kernel radius for models neglecting the evolution of the kernel temperature. The final critical radius, based on the flame front thickening R_c, is much smaller than the critical radius based on the turbulent length scale of the external turbulence R_b, illustrated in Figures 3 and 6, indicating that the limiting factor for the quenching is the external turbulent field, and not the turbulence generated by the flame front.
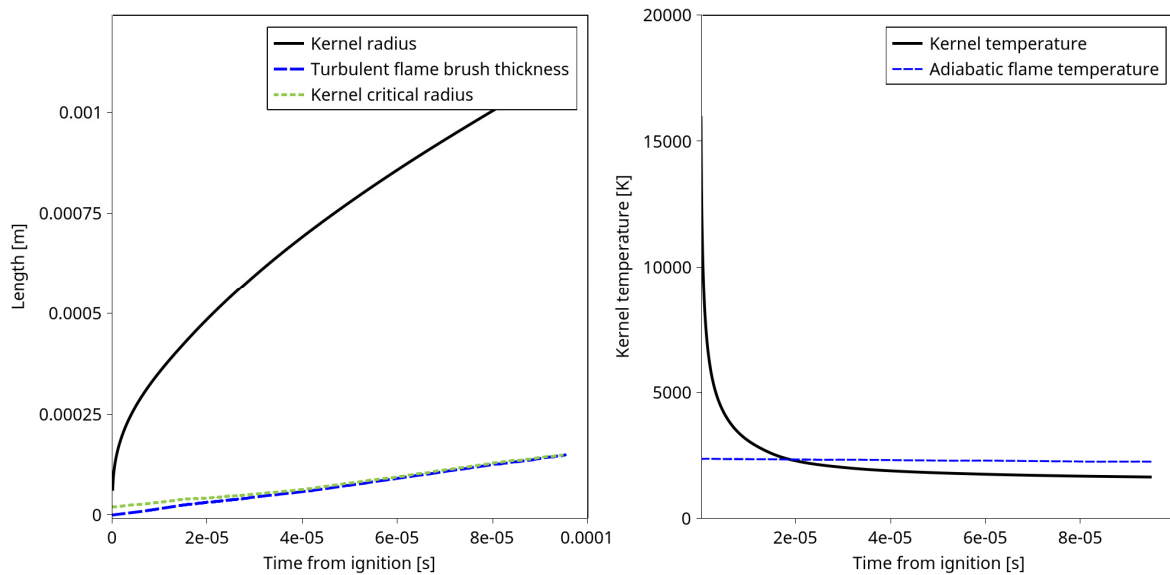

Figure 7: Kernel evolution for the baseline model parameters, (injected mass m=0.9mg)

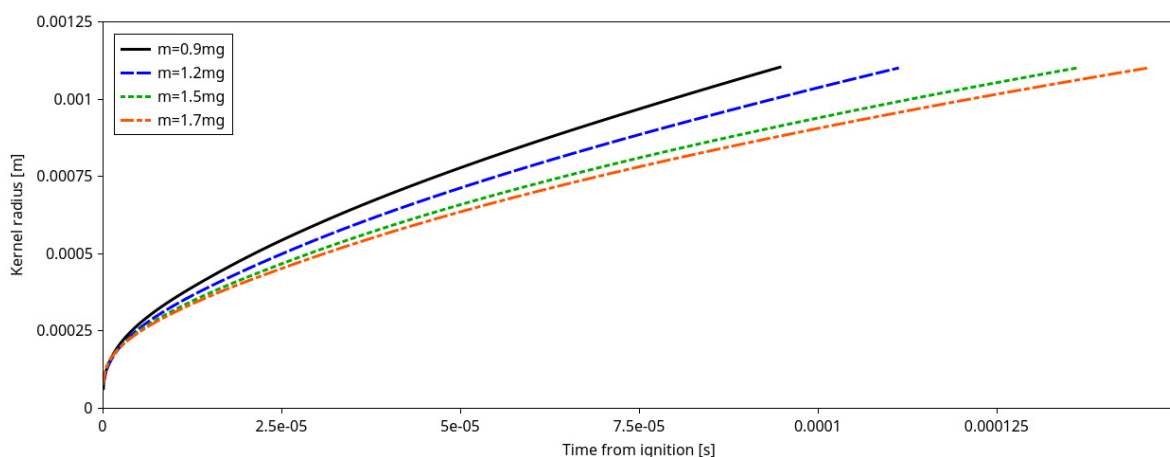The speed of the flame kernel growth follows the composition of the mixture in the spark region as shown in Figure 8.

Figure 8: Kernel evolution for the baseline model parameters, (injected mass m=0.9mg)

The flame jet exit time obtained in the simulations and the comparison with the experimental data are summarized in Table 6. The jet exit times were determined in the

simulation by calculating the time at which the concentration of the burnt fuel in the mass flow rate through the outlets of pre-chamber nozzles reaches 4.5%.

The time was then averaged between the nozzles. Tests with various thresholds showed low sensitivity to the threshold value (see [13] for more detail). Experimental jet exit times are determined by the threshold in OH* chemiluminescence levels. It is difficult to compare the two levels directly. However, the indication of the agreement is the offset between the two values, which is constant apart from the outlier 1.5mg injection, which also shows a local maximum in the standard deviation of the experimental results.

Table 6: Flame jet exit timings for baseline set-up

Injected mass (mg)	Experiment		Simulation	
	Flame jet exit time (ms)	Standard deviation (%)	Flame jet exit time (ms)	Difference vs experiment (%)
0.9	0.75	11.3	0.58	22.6
1.2	0.81	12.5	0.60	23.5
1.5	0.94	15.5	0.66	30.0
1.7	0.88	9.8	0.68	22.7

The results reported in Table 6 show higher deviation from the experimental data than the results reported in [22], where a different experimental set-up was considered with a much shorter injection duration. Note that results reported in [22] were obtained with the effective spark power of 180W and transition radius of 4mm, in effect delaying the flame development.

Simulation of cases with varying number of particles demonstrated that the flame jet exit times exhibit no sensitivity to kernel. For example, the variation of the maximum of recorded flame jet exit time between the nozzles, when changing the number density from 20000 to 1000 particles was equal to 0.06% for the baseline case with 0.9 injected mass. The critical gas phase Courant number for the initial stage of the kernel growth comprising the first ~20µs during which the temperature relaxes to adiabatic flame temperature was found to be equal to 0.1. While the model would still converge, increasing time step beyond this value resulted in a sharp unphysical decrease of the kernel temperature. After this initial stage, the model was found to be stable with the gas phase Courant number of up to 2.

The increase in the breakdown energy leads to the increase in the initial flame kernel size, which results in faster cooling of the kernel due to a higher initial surface area. The current implementation of the model explicitly restricts the contraction of the kernel, hence this slower initial growth still leads to the same values of the kernel radius at later times (Figure 9).
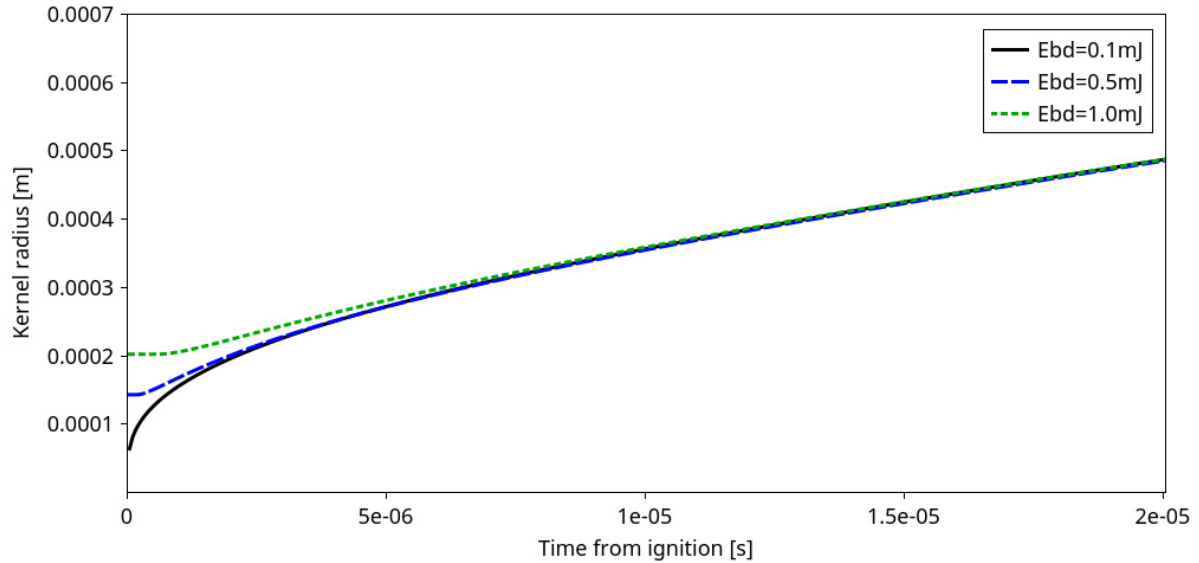
Figure 9: Effect of the breakdown energy on the kernel growth (injected mass m=0.9mg)

Within the 1D model context, increase of the transition radius is equivalent to an extension of the duration of the 1D stage. Extended duration of the 1D model slows down the development of the flame and increases the flame jet exit time. The decrease of the effective power has the same effect; hence it is useful to consider the two together. Figure 10 shows the burned fuel mass fraction in the mass flow rate through one of pre-chamber nozzles (there was no substantial asymmetry observed between the nozzles). The variation of the transition radius for the same spark within the limits suggested in [10] does not have a strong effect on the flame jet exit time. However, the effective spark power change within the 210W-1W range changes the jet exit time by 0.31ms (1.1deg).
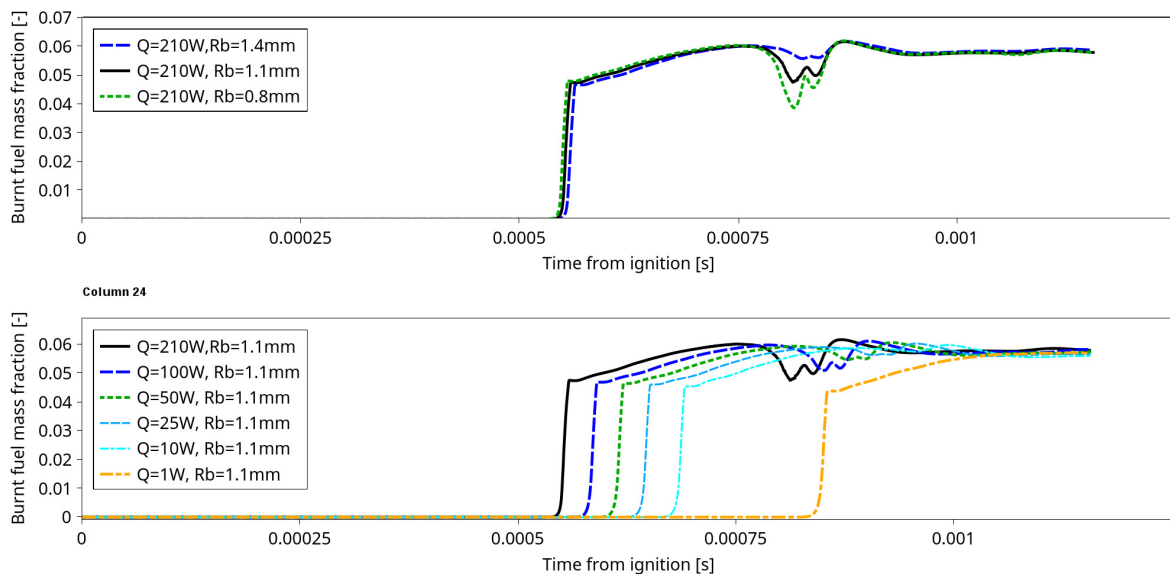

Figure 10: Effect of the effective power and transition radius on flame propagation (injected mass m=0.9mg)

The effective spark power in the range 180-210W, has been shown to produce correct results when compared with the experiments of Maly [15] ([5, 13]), with a different coil. The same set-up also showed good results when compared with the measurements done in the optical engine for a similar coil/spark combination [5]. While some variation in the effective power depending on ambient pressure, density and spark coil properties can be expected, the values of the effective power ~5W required to close the gap with the experimentally observed flame jet exit times are not realistic.

5   Conclusions

The Dynamic Discrete Particle Ignition Kernel has been designed and implemented within the VECTIS software product as part of the Horizon 2020 GasOn project. This model has been successfully validated against academic test cases in other published works and here the model is used within a Rapid Expansion Compression Machine environment.

The results have shown that there can be some variation between simulation results and those from measurements when comparing the time taken for an ignition event to travel from the spark through the pre-chamber and into the main combustion chamber. The implemented ignition model has several input parameters which are subject to uncertainty. Here these parameters have been investigated to examine the effect that they have on this discrepancy between the flame jet timings.

The sensitivity to the number of particles used in the DDPIK model is slight, with a reduction from 20000 to 1000 producing only a 0.06% change in the results. The reduction in the number of particles being tracked also results in a reduction in computational cost, improving the model for industrial applications and time frames. Variation of the transition timing for the same spark energy also produces small variations and does not produce as strong effect on the flame jet exit timing. The results are sensitive to the effective spark power input parameter. However the variation of the effective spark power input within reasonable limits does not allow closing the gap with the experimentally observed flame jet timings.

The dynamic discrete particle ignition model shows good robustness and accuracy over a range of air-fuel ratios. The sensitivity analysis of model parameters conducted here indicates that the uncertainties in the spark model alone cannot account for the faster flame propagation apparently observed by comparison with the experiment. The model is robust and can be used with the default settings established in [5.13].

The only remaining factor which can affect the flame jet exit time is the turbulent flame speed closure used in the G-equation part of the combustion model. In particular, the value of the coefficient A used in Equation 5 has been reported to be sensitive to flow conditions and turbulence levels [13, 23, 24].

The effect of the turbulent flame speed on the simulations of the RCEM experiment are explored in detail in the following publication [13].

Acknowledgements

Bibliography

[1]   Christof Schernus, RD., Knut Habermann, BGP. "Potentials of gas mobility in road transport", BDEW-Fachkongress 2016. Berlin 2016-03-02

[2]   Möhring, L., Andersen, J.: "CNG Mobility - Scalable, Affordable and Readily Available Solution for Environmental and Climate Challenges" 38. Internationales Wiener Motorensymposium 2017

[3]   Ferrera, M., "Gas-Only Internal Combustion Engines, H2020GV-3-2014 Future natural gas powertrains and components for cars and vans". NGVA – Clean future with g-mobility. Paris. 25 May 2018,

[4]   Lucas, G., Tallu, G. and Weißner, M., "CFD-based Development of an Ignition Chamber for a lean and highly efficient CNG Combustion", Proc. THIESEL 2018 Conference on Thermo- and Fluid Dynamic Processes in Direct Injection Engines, 2018.

[5]   Tallu, G., Beck, L. M., Prouvier, M., Winkler, A. and Shapiro, E., "3D CFD Modelling and Simulation of Spark Ignition Inclusive of Turbulence Effects and Detailed Chemical Kinetics", Proc. 3rd International Conference on Ignition Systems for Gasoline Engines, November 3–4, 2016, Berlin

[6]   Tallu G., Frambourg M., Prouvier M., Weißner M., Winkler A., "Numerical Investigation of Spark Ignition Processes in Natural Gas Engines with the Advanced Spark Ignition Model", Proc. 4th International Conference on Ignition Systems for Gasoline Engines, Berlin, December 2018

[7]   Sher, E., Ben-Yaish, J. and Kravchik, T., "On the birth of spark channels", Combustion and Flame, 89:168-194, 1992.

[8]   Refael S. and Sher E., "A theoretical study of the ignition of a reactive medium by means of an electrical discharge", Combustion and Flame, 59:17-30, 1985.

[9]   Rivin B., Dulger M. and Sher E., "Extending Lean Misfire Limit of Methane-Air Mixtures by Means of an Enhanced Spark Discharge", SAE - 1999-01-0573

[10]   Tan, Z. and Reitz, R. "Modeling ignition and combustion in spark-ignition engines using a level set method", SAE Technical Paper 2003-01-0722, 2003.

[11]   Herweg R. and Maly, R. R. "A fundamental model for flame kernel formation in S.I. engines". In SAE International, 922243, 1992.

[12]   Maly R.R., "Spark Ignition, its Physics and Effect on the Internal Combustion Process", in Fuel Economy: Road Vehicles Powered by Spark Ignition Engines, ed. by J.C. Hilliard, G.S. Springer, Plenum Press, New York 91–148 (1984).

[13]   Shapiro E., Kyrtatos P., Kotzagianni M., Bolla M., Tiney N., Boulouchos K., "Experimental and numerical analysis of pre-chamber combustion systems for lean

burn gas engines", Submitted to SAE World Congress and Exhibition, Manuscript no: 19PFL-0579

[14] Bolla M., Shapiro E., Tiney N., Kyrtatos P., Kotzagianni M., Boulouchos K., "Numerical study of turbulence and fuel-air mixing within a scavenged pre-chamber using RANS and LES", Submitted to SAE World Congress and Exhibition, Manuscript no: 19PFL-0664

[15] Maly, R. and Vogel, M., "Initiation and propagation of flame front in lean ch4-air mixture by the three modes of the ignition spark", Proceedings of the 17th Symposium (international) on Combustion, The Combustion Institute, 17, pp. 821-831, 1978.

[16] Maly R.R., Herweg R. "Spark Ignition and Combustion in Four-Stroke Gasoline Engines". In: Arcoumanis C., Kamimoto T. (eds) Flow and Combustion in Reciprocating Engines. Experimental Fluid Mechanics. Springer, Berlin, Heidelberg, 2008

[17] Miles P. C., RempelEwert B. H., Reitz R. D., "Experimental Assessment of Reynolds-Averaged Dissipation Modeling in Engine Flows", SAE-2007-24-0046

[18] Lipatnikov, A.N. and Chomiak, J. "Turbulent Flame Speed and Thickness: Phenomenology, Evaluation, and Application in Multi-Dimensional Simulations", Progress in Energy and Combustion Science, 28, No. 1, pp. 1-73, 2002

[19] Ewald, J. and Peters, N., "On unsteady premixed turbulent burning velocity prediction in internal combustion engines.", Proceedings of the Combustion Institute, 31:3051–3058, 2007.

[20] Stiesch G, Merker GP, "A Simplified Model for Description of Triple Flames in Stratified Charge Gasoline Engines", in: Proc 12th Int. Multidim. Engine Modeling, Users Group Meeting, Detroit, MI, 2002.

[21] Przulj, V., Tiney, N., Shapiro, E., Penning, R. and Shala, M., "The time scale bounded k-e turbulence model and its assessment for automotive applications", Proc. 7th Int. Symp. Turbulence, Heat and Mass Transfer, Palermo, Italy, 2012

[22] Hernández, I., Shapiro, E., Tiney, N., Kotzagianni, M., Kyrtatos, P. and Boulouchos, K., "Flame-wall interaction modelling for pre-chamber combustion in lean burn gas engines", Proceedings of 34th International CAE Conference and Exhibition, 2018, Vicenza, Italy

[23] Schmitt M., Hu, R., Wright, Y. M., Soltic P. and Boulouchos K. "Multiple Cycle LES Simulations of a Direct Injection Methane Engine," Flow, Turbulence and Combustion (95):645–668, 2015

[24] Xu, G., Hanauer, C., Wright, Y., and Boulouchos, K., "CFD-Simulation of Ignition and Combustion in Lean Burn Gas Engines", SAE Technical Paper 2016-01-0800, 2016, doi:10.4271/2016-01-0800

[25] Kammermann T., Kreutner W., Trottmann M., Merotto L., Soltic P., Bleinera D., "Spark-induced breakdown spectroscopy of methane/air and hydrogenenriched methane/air mixtures at engine relevant conditions", Spectrochimica Acta Part B 148, pp. 52–164, 2018